AIAA JOURNAL
Vol. 46, No. 9, September 2008

Boundary Conditions for Acoustic Eigenmode Computations in Gas Turbine Combustion Chambers

N. Lamarque*
Centre Européen de Recherche et de Formation Avancée en Calcul Scientifique, 31057 Toulouse, France
and
T. Poinsot†
Institut de Mécanique des Fluides de Toulouse, 31400 Toulouse, France

DOI: 10.2514/1.35388

Understanding and predicting acoustic instabilities in gas turbine combustion chambers requires the knowledge of the acoustic behavior of all the elements feeding the combustion chamber (characterized by their impedance). Inlets and outlets of chambers are often represented as one-dimensional ducts and existing methods to evaluate impedances of choked and unchoked nozzles are described: 1) analytical formulas, 2) numerical methods using the linearized Euler equations and a finite dfference solver in Fourier space and 3) full space–time solver in which the response of the nozzle is studied by forcing its inlet (or outlet) and measuring its response in the time domain. These three methods are compared in reference cases (a straight duct and a subsonic distributor). Practical implications for gas turbines are then discussed. In such cases, if the diffusers and distributors connected to the chamber are not choked, it is shown that solving the acoustic problem becomes very difficult because compressor and turbine impedances are usually not known. This paper finally shows how these impedances control the acoustic oscillations of a combustion chamber by presenting an example of acoustic eigenmode calculations in a realistic gas turbine, using a Helmholtz solver and various impedances for the inlet and outlet of the combustor.

Nomenclature

A	=	section, m^2
$\mathcal{A}$	=	acoustic-wave amplitude, Pa
$[A]$, $[C]$	=	$N \times N$ real matrices
$[B]$	=	$N \times N$ complex matrix
c	=	sound speed, m/s
c_p	=	mass specific heat capacity for constant pressure, J/kg/K
c_v	=	mass specific heat capacity for constant volume, J/kg/K
$[D]$	=	2×2 invertible matrix
f	=	frequency, Hz
g_1	=	real-valued function
g_2	=	real-valued function
h	=	space step, m
K	=	real constant
k	=	wave number, rad/m
L	=	nozzle length, m
$\dot{m}$	=	mass flow rate, kg/m^{-3}
N	=	number of discretization nodes
$\mathbf{n}$	=	unit normal vector
p	=	pressure, Pa
p_t	=	total pressure, Pa
$\{p'\}$	=	acoustic pressure amplitude N vector
R	=	reflection coefficient
r	=	molar perfect-debs-gas constant, J/mol/K
s	=	entropy, J/kg/K
T	=	temperature, K
T	=	transmission coefficient
t	=	time, s
W	=	molar mass, kg/mol
W_{ac}	=	total acoustic energy flux
$\mathbf{x}$	=	position vector
Y	=	reduced acoustic admittance
Z	=	reduced acoustic impedance
Δ_0	=	second-order central differences
δ	=	adimensionalized volume mass fluctuation
δ^-	=	first-order upwind differences
γ	=	polytropic gas constant
λ	=	wave length, m
ν	=	adimensionalized velocity fluctuation
ρ	=	volume mass, kg/m^3
ϕ	=	real-valued function
φ	=	adimensionalized pressure fluctuation
Ω	=	computational domain
Ω'_T	=	heat release amplitude, rad/s
ω	=	angular frequency, rad/s
$(\cdot)'$	=	fluctuating values
$\bar{(\cdot)}$	=	mean values

Subscripts

x	=	x-axis value
y	=	y-axis value
1	=	upstream value
2	=	downstream value

Superscripts

I	=	incident wave
(j)	=	discretization index
R	=	reflected wave
ϵ	=	parameter
$+$	=	downstream traveling wave
$-$	=	upstream traveling wave

Received 30 October 2007; revision received 25 March 2008; accepted for publication 21 May 2008.

*Postdoctoral Fellow.
†Research Director. Associate Fellow AIAA.

I. Introduction

COMBUSTION instabilities (CI) are an important research theme for the gas turbine industry [1]. The central role played

by acoustics in many combustion instability scenarios has long been the subject of controversies, but is now more and more widely recognized. Two classes of methods can be used today to study oscillations in combustors [2–6].

Large eddy simulation (LES) is becoming a standard tool to study the stability of many modern combustion devices such as aero or industrial gas turbines, rocket engines, or industrial furnaces. When LES is performed using compressible Navier–Stokes equation solvers, it directly provides both the time-resolved flow and the acoustic field. Multiple recent papers have demonstrated that LES accurately predicts mean flowfields in turbulent combustors [7–10]. Other studies [11–13] show that LES of compressible flows also correctly predicts the acoustic fluctuations in turbulent combustors and therefore can be used to study CI. However, a major drawback of LES remains its cost, especially when describing compressible flows (small time steps). Moreover, extracting an acoustic mode from a turbulent flow is a hard task, which increases the difficulty to point out the phenomena that control the appearance of CI.

Because LES remains expensive, developing alternative approaches is an interesting path: studying the linear stability of combustors is the most obvious method. This is usually achieved by Helmholtz codes, which solve the linearized wave equation to predict the frequencies and the growth rates of the acoustic modes of the combustor [2,4,5,14,15]. These codes run much faster than LES and work in the frequency domain, whereas LES works in the time domain. They rely on crude modeling assumptions for the base flow (which is often supposed to be the mean flow) and for the effect of the flame on the acoustic field (using a flame transfer function). They are well suited to parametric studies: for example, to optimize damping devices or combustion chamber shapes which minimize oscillations.

Both compressible LES and Helmholtz solvers naturally include acoustics and will correctly give acoustic fields provided that crucial and often forgotten information is available: the acoustic impedances of all inlets, outlets, and walls.[‡] In real engines, the combustion chamber is fed by a diffuser and flows into a distributor (Fig. 1). A central question to evaluate impedances is to know which elements of the engine really determine the impedance of the diffuser and of the distributor. The latter are usually choked, and so most authors consider that the throat is a proper place to specify acoustic boundary condition. However, in certain cases, distributors are not choked (during startup, for example, during which instabilities are often observed), and in most cases, diffusers are not choked. For those situations, the evaluation of impedances can become a critical issue. The objectives of this paper are as follows:

1) Review analytic methods to evaluate impedances of one-dimensional ducts and extend the approach of Marble and Candel [17].

2) Present a tool able to predict the impedance of combustor inlets and outlets by approximating them as nozzle flows.

3) Give simple academic examples of impedance calculations.

4) Discuss the conditions that allow an evaluation of the impedances of a real gas turbine, taking into account only the geometry of the diffuser and distributor as well as the mean flow.

5) Present an example of the importance of inlet and outlet impedances in the computation of modes in a real gas turbine chamber.

Reduced acoustic impedances measure the ratio between the fluctuations of acoustic pressure and velocity at a given frequency:

$$Z(\omega) = \frac{p'}{\bar{\rho}\,\bar{c}\,\mathbf{u}'\cdot\mathbf{n}} \tag{1}$$

Impedance is a complex-valued function of ω. In fluids at rest, its real part is closely linked to the acoustic energy flux $p'\mathbf{u}'$ (a zero real part means the acoustic flux is zero, because pressure and velocity have opposite phases) [6]. It is well known in some particular cases that $Z = 1$ for an infinitely long duct, $Z = 0$ for an outlet at constant pressure, and $Z \to \infty$ on a rigid wall. In the last relation, impedance is often replaced by its inverse, called admittance, and is defined as $Y = 1/Z$.

[‡]Rigid walls obviously correspond to simple zero-velocity conditions that are simple to implement, but gas turbine chambers often use multiperforated walls to cool the combustion chamber and these walls have complex impedances [16]. Multiperforated walls are not considered here.

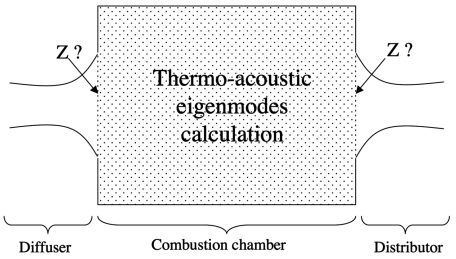

Fig. 1 Combustion chamber with diffuser and distributor. Ducts feeding the chamber are replaced by acoustic impedances for the eigenmode calculation.

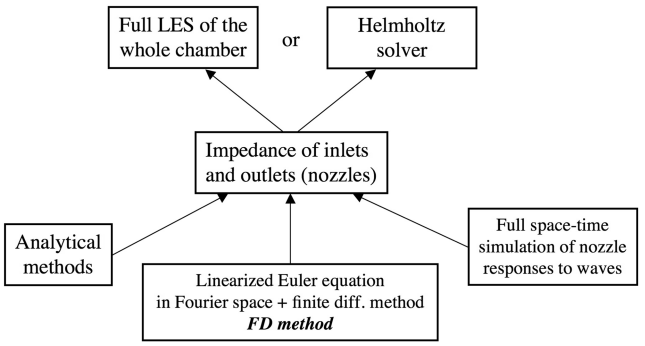

Fig. 2 Connections between the different calculations needed to study the thermoacoustic stability of combustion chambers.

There are three main methods to evaluate impedances (Fig. 2). First, in simple cases and at low frequencies, analytical formulations may be available [17,18] and are described in Sec. II. Second, for cases in which the geometry of the considered component (diffuser or distributor) becomes complex and the frequency is not low, the one-dimensional Euler equations can be linearized around the mean state. Impedances at one end of the duct can be obtained as a function of the geometry only if the flow is choked or as a function of the geometry and the impedance at the other side of the component if the flow remains subsonic. Such methods (here, called the FD method, because a finite difference solver is required to solve the linearized equations in Fourier space) are presented in Sec. III.C. Third, a space–time solver (Euler equations for compressible flows) can also be used to force the component with harmonic waves and measure its response in terms of impedances in the time domain. This method is expensive; it is described briefly in Sec. V and used here as a reference technique to evaluate the precision of the FD method. Finally, Sec. VII illustrates the role of impedances (or admittances); the principles of Helmholtz solvers are briefly described and the influence of the boundary conditions is highlighted in the case of a gas turbine chamber, including all parts (casing, swirler, combustion chamber, dilution holes, and choked outlet nozzle).

II. Analytical Formulations for Impedances of Compact Nozzles

For low frequencies, several analytical formulations for reflection coefficients or impedances were developed for simplified cases. Despite strong hypotheses, they remain accurate, even when nonlinear effects occur [19]. The acoustic waves are considered here as plane waves because their wavelengths are large in comparison with the characteristic lengths of the ducts. The general form of acoustic pressure and velocity in constant-section ducts can be written [6,17]

$$\frac{p'}{\gamma\bar{p}} = \mathcal{A}^+\exp(ik^+x - i\omega t) + \mathcal{A}^-\exp(-ik^-x - i\omega t) \tag{2}$$

$$\frac{u'}{\bar{c}} = \mathcal{A}^+ \exp(ik^+x - i\omega t) - \mathcal{A}^- \exp(-ik^-x - i\omega t) \qquad (3)$$

where $k^+ = \omega/(\bar{c} + \bar{u})$ and $k^- = \omega/(\bar{c} - \bar{u})$. Determining the acoustic boundary conditions requires the determination of an impedance as defined by Eq. (1) or a reflection coefficient R, given by

$$R = \frac{\mathcal{A}^R}{\mathcal{A}^I} \qquad (4)$$

The relation between R and Z depends on the orientation of $\mathbf{n}$. For $\mathbf{n}$ pointing toward positive abscissas, it is written

$$R = \frac{Z-1}{Z+1} \qquad (5)$$

The simplest approximation has been described by Rienstra [20], who showed that the reflection coefficient of an open outlet is -1 (or zero impedance) for zero Strouhal number flows. This simplification can be used for academic experimental setups, but in the context of gas turbines, its application remains limited because combustion chambers rarely flow into open atmosphere, but into high-pressure stators followed by turbines.

A first approach to determine reflection coefficients or impedances of these passages is to consider them as compact nozzles (Fig. 3), as proposed by Marble and Candel [17] and Candel [18]. When the characteristic scale of the fluctuations is large compared with the duct length (i.e., $\lambda \gg L$), the duct can be seen as a discontinuity in the wave propagation. Thus, it is not necessary to solve the flow in the duct and its influence can be replaced by matching conditions (built in the same way as jump conditions through a shock wave) [17]. For example, in the distributor following the combustion chamber of aircraft, a typical length scale is 10 cm (the length of the distributors vanes). For burned gases at 1200 K with a sound speed of 700 m/s, a reasonable compactness condition ($\lambda \approx 10L$) leads to a critical frequency f_c of the order of 700 Hz; the distributor nozzle can then be considered as compact for all frequencies up to 700 Hz. Marble and Candel [17] used conservation laws in subsonic and choked compact nozzles to derive reflection coefficients. The conservation of mass flow ($\dot{m} = \rho u A$) between inlet (side 1) and outlet (side 2) can be written

$$\dot{m}_1 = \dot{m}_2 \qquad (6)$$

If there is neither heat loss nor normal shock, the total temperature, defined by $T_t = T(1 + [(\gamma-1)/2]M^2)$, with $M = u/c$, is also conserved between side 1 and side 2 and leads to

$$T_{t,1} = T_{t,2} \qquad (7)$$

The two conservation equations (6) and (7) imply that

$$\frac{\dot{m}'_1}{\bar{\dot{m}}_1} = \frac{\dot{m}'_2}{\bar{\dot{m}}_2} \quad \text{and} \quad \frac{T'_{t,1}}{\bar{T}_{t,1}} = \frac{T'_{t,2}}{\bar{T}_{t,2}} \qquad (8)$$

with

$$\frac{\dot{m}'}{\bar{\dot{m}}} = \frac{1}{\bar{M}}\frac{u'}{\bar{c}} + \frac{\rho'}{\bar{\rho}} \qquad (9)$$

and

$$\frac{T'_t}{\bar{T}_t} = \frac{1}{1 + [(\gamma-1)/2]\bar{M}^2}\left[\gamma\left(\frac{p'}{\gamma\bar{p}}\right) - \frac{\rho'}{\bar{\rho}} + (\gamma-1)\bar{M}\frac{u'}{\bar{c}}\right] \qquad (10)$$

A. Choked Distributor

If the distributor is choked, and if the frequency of perturbations is low, the flow rate can be assumed to match its choked value at all times. The mass flow rate is then directly linked to the thermodynamic state upstream of the nozzle:

$$\dot{m} = \frac{p_{t,1}}{\sqrt{\gamma r T_{t,1}}} A_* \gamma \left(\frac{\gamma+1}{2}\right)^{-\frac{\gamma+1}{2(\gamma-1)}} \qquad (11)$$

where $p_{t,1} = p_1(1 + [(\gamma-1)/2]M_1^2)^{\frac{\gamma}{\gamma-1}}$ is the total pressure upstream of the nozzle (Fig. 3). The logarithmic derivative of $\dot{m}_1$ can be calculated from Eq. (11) using the fractional variation of total pressure at side 1,

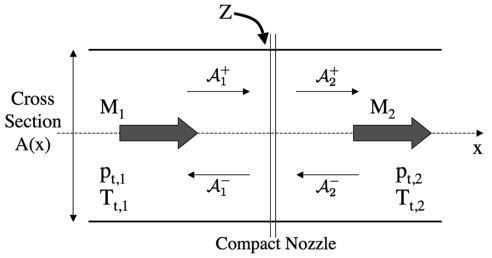

Fig. 3 Compact nozzle modeled as a discontinuity between the upward and downward flows.

$$\frac{p'_{t,1}}{\bar{p}_{t,1}} = \frac{1}{1 + [(\gamma-1)/2]\bar{M}_1^2} \times \left[\gamma\left(1 - \frac{1}{2}\bar{M}_1^2\right)\left(\frac{p'_1}{\gamma\bar{p}_1}\right) + \gamma\bar{M}_1\frac{u'_1}{\bar{c}_1} + \frac{1}{2}\gamma\bar{M}_1^2\frac{\rho'_1}{\bar{\rho}_1}\right] \qquad (12)$$

and Eq. (10) written at side 1. This leads to[§]

$$\frac{\dot{m}'_1}{\bar{\dot{m}}_1} = \frac{p'_{t,1}}{\bar{p}_{t,1}} - \frac{1}{2}\frac{T'_{t,1}}{T_{t,1}} = \frac{1}{1 + [(\gamma-1)/2]\bar{M}_1^2} \times \left[\frac{\gamma}{2}(1 - \bar{M}_1^2)\left(\frac{p'_1}{\gamma\bar{p}_1}\right) + \frac{\gamma+1}{2}\bar{M}_1\frac{u'_1}{\bar{c}_1} + \frac{1}{2}(1 + \gamma\bar{M}_1^2)\frac{\rho'_1}{\bar{\rho}_1}\right] \qquad (13)$$

Then combining Eq. (9) written at side 1 and Eq. (13) entails

$$\frac{u'_1}{\bar{u}_1} = \frac{1}{2}\frac{T'_1}{\bar{T}_1} \quad \text{or} \quad \frac{u'_1}{\bar{c}_1} - \frac{\gamma}{2}\bar{M}_1\left(\frac{p'_1}{\gamma\bar{p}_1}\right) + \frac{1}{2}\bar{M}_1\frac{\rho'_1}{\bar{\rho}_1} = 0 \qquad (14)$$

which is equivalent to write that the fluctuating Mach number is zero:

$$M'_1 = \bar{M}_1\left(\frac{u'_1}{\bar{u}_1} - \frac{1}{2}\frac{T'_1}{\bar{T}_1}\right) = 0$$

Supposing that there is no incoming entropy wave $s'_1 = 0$, so that $\rho'_1/\rho_1 = p'_1/\gamma\bar{p}_1$, Eq. (14) leads to an expression for the acoustic inlet impedance:

$$Z_1 = \frac{2}{\bar{M}_1(\gamma-1)} \quad \text{hence } R_1 = \frac{\mathcal{A}_1^-}{\mathcal{A}_1^+} = \frac{1 - \frac{1}{2}(\gamma-1)\bar{M}_1}{1 + \frac{1}{2}(\gamma-1)\bar{M}_1} \qquad (15)$$

$\mathcal{A}_1^-$ does not depend on the downstream flow because no wave can come from downstream of the throat. Equation (15) also shows that a choked nozzle behaves nearly like a rigid wall ($R = 1$) for low upstream Mach number ($M_1 \to 0$), which is a commonly used boundary condition for choked nozzles.

B. Choked Diffuser

The case of a choked diffuser is particular. Diffusers generally disembogue in a chamber casing or a plenum, in which the flow is subsonic; if the diffuser is choked, there is also a shock between its throat and its outlet. Stow et al. [21] presented an analysis of the acoustic response of a choked diffuser with a normal shock in the expansion part of the duct. Assuming there is no disturbance coming from upstream ($\mathcal{A}_1^+ = 0$), they showed that

$$R_2 = \frac{1 - \gamma\bar{M}_2 + (\gamma-1)\bar{M}_2^2}{1 + \gamma\bar{M}_2 + (\gamma-1)\bar{M}_2^2} \qquad (16)$$

A generalization for transmission coefficients was also derived by Moase et al. [22], assuming there can be perturbation upstream of the shock and $\mathcal{A}_1^+$ is known.

C. Unchoked Distributor/Diffuser

In the case of a subsonic flow in the nozzle, information can propagate in both directions. Thus, information on the other side of the duct is needed to determine reflection coefficients. Conservation of mass flow rate and total temperature [Eq. (8) with Eqs. (9) and (10)] are used to write a system of 2 equations with 6 unknowns: u'_1,

[§]This relation can also be written at side 2, but this is of no interest here.

u'_2, ρ'_1, ρ'_2, p'_1, and p'_2. Supposing again that there is no entropy wave ($s'_1 = s'_2 = 0$) to eliminate ρ'_1 and ρ'_2 gives the following system of 2 equations with 4 unknowns:

$$\frac{1}{\bar{M}_1}\frac{u'_1}{\bar{c}_1} + \frac{p'_1}{\gamma \bar{p}_1} = \frac{1}{\bar{M}_2}\frac{u'_2}{\bar{c}_2} + \frac{p'_2}{\gamma \bar{p}_2} \tag{17}$$

$$\frac{1}{1+[(\gamma-1)/2]\bar{M}_1^2}\left[\frac{p'_1}{\gamma \bar{p}_1} + M_1\frac{u'_1}{\bar{c}_1}\right] = \frac{1}{1+[(\gamma-1)/2]\bar{M}_2^2}\left[\frac{p'_2}{\gamma \bar{p}_2} + M_2\frac{u'_2}{\bar{c}_2}\right] \tag{18}$$

Writing pressure and velocity perturbations as waves [Eqs. (2) and (3) in Eqs. (17) and (18)] gives

$$\frac{1}{\bar{M}_1}(\mathcal{A}_1^+ - \mathcal{A}_1^-) + \mathcal{A}_1^+ + \mathcal{A}_1^- = \frac{1}{\bar{M}_2}(\mathcal{A}_2^+ - \mathcal{A}_2^-) + \mathcal{A}_2^+ + \mathcal{A}_2^- \tag{19}$$

$$\frac{1}{1+[(\gamma-1)/2]\bar{M}_1^2}[\mathcal{A}_1^+ + \mathcal{A}_1^- + \bar{M}_1(\mathcal{A}_1^+ - \mathcal{A}_1^-)] = \frac{1}{1+[(\gamma-1)/2]\bar{M}_2^2}[\mathcal{A}_2^+ + \mathcal{A}_2^- + \bar{M}_2(\mathcal{A}_2^+ - \mathcal{A}_2^-)] \tag{20}$$

If the outlet reflection coefficient $R_2 = \mathcal{A}_2^-/\mathcal{A}_2^+$ of the distributor is known, system (19) and (20) gives the reflection coefficient at the inlet,

$$R_1 = \frac{\mathcal{A}_1^-}{\mathcal{A}_1^+} = \frac{\bar{M}_1+1}{\bar{M}_1-1}\frac{(\bar{M}_1-\bar{M}_2)(\bar{M}_2+1)(1-[(\gamma-1)/2]\bar{M}_1\bar{M}_2) + (\bar{M}_1+\bar{M}_2)(\bar{M}_2-1)(1+[(\gamma-1)/2]\bar{M}_1\bar{M}_2)R_2}{(\bar{M}_1+\bar{M}_2)(\bar{M}_2+1)(1+[(\gamma-1)/2]\bar{M}_1\bar{M}_2) + (\bar{M}_1-\bar{M}_2)(\bar{M}_2-1)(1-[(\gamma-1)/2]\bar{M}_1\bar{M}_2)R_2} \tag{21}$$

whereas the transmission coefficient is [17]

$$\mathsf{T}_1 = \frac{\mathcal{A}_2^+}{\mathcal{A}_1^+} = \frac{2\bar{M}_2}{1+\bar{M}_2}\frac{(\bar{M}_1+1)(1+[(\gamma-1)/2]\bar{M}_2^2)}{(\bar{M}_1+\bar{M}_2)(1+[(\gamma-1)/2]\bar{M}_1\bar{M}_2)} \tag{22}$$

The same derivation for a diffuser gives R_2 as a function of $R_1 = \mathcal{A}_1^+/\mathcal{A}_1^-$,

$$R_2 = \frac{\mathcal{A}_2^+}{\mathcal{A}_2^-} = \frac{1-\bar{M}_2}{\bar{M}_2+1}\frac{(\bar{M}_2-\bar{M}_1)(\bar{M}_1-1)(1-[(\gamma-1)/2]\bar{M}_1\bar{M}_2) + (\bar{M}_1+\bar{M}_2)(1+\bar{M}_1)(1+[(\gamma-1)/2]\bar{M}_1\bar{M}_2)R_1}{(\bar{M}_1+\bar{M}_2)(1-\bar{M}_1)(1+[(\gamma-1)/2]\bar{M}_1\bar{M}_2) + (\bar{M}_1-\bar{M}_2)(1+\bar{M}_1)(1-[(\gamma-1)/2]\bar{M}_1\bar{M}_2)R_1} \tag{23}$$

and the transmission coefficient is [17]

$$\mathsf{T}_2 = \frac{\mathcal{A}_1^-}{\mathcal{A}_2^-} = \frac{2\bar{M}_1}{1-\bar{M}_1}\frac{(1-\bar{M}_2)(1+[(\gamma-1)/2]\bar{M}_1^2)}{(\bar{M}_1+\bar{M}_2)(1+[(\gamma-1)/2]\bar{M}_1\bar{M}_2)} \tag{24}$$

Those results, summarized in Table 1, generalize the formulas given by Marble and Candel [17]; for $R_2 = 0$, Eq. (21) is identical to their results, whereas Eq. (23) matches their results when $R_1 = 0$. A similar work, introducing entropy disturbances, was recently done by Moase et al. [22].

III. Numerical Evaluation of Impedances Using the Linearized Euler Equations

The hypothesis of compacity is only applicable when the acoustic-wave length is much larger than the nozzle length. This is too strict an approximation as soon as perturbation frequencies become large. The problem must then be solved in more detail; for example, mean flow and then fluctuating pressures and velocities have to be calculated in the duct.[¶] The first consequence of taking finite length ducts into account is that impedances now depend on frequency, which is a major improvement in comparison with the previous approximations.

The inlet impedance (or outlet impedance) of a distributor (diffuser) can be obtained by solving the linearized Euler equations under some assumption: the mean flow in these ducts is quasi-one-dimensional and isentropic, all geometrical complexities are included in the one-dimensional cross-sectional evolution of the inlet or outlet ducts (which are described like simple nozzles), and, finally, the flow is a perfect gas with constant composition (no chemistry) and constant heat capacities. With these assumptions, the Euler equations are written

$$\frac{\partial \rho A}{\partial t} + \frac{\partial \rho u A}{\partial x} = 0 \tag{25}$$

$$\frac{\partial u}{\partial t} + u\frac{\partial u}{\partial x} + \frac{1}{\rho}\frac{\partial p}{\partial x} = 0 \tag{26}$$

$$\frac{\partial s}{\partial t} + u\frac{\partial s}{\partial x} = 0 \tag{27}$$

The system is completed by the equation of state for perfect gas: $p = \rho\frac{R}{W}T$.

A. Acoustics in a Nozzle

For the linearization of system (25–27) [17,18,23,24], the variables (velocity, pressure, or density) are first decomposed in two parts: a mean component (overbarred values), which only varies with space coordinates, and a small fluctuating component (primed values), which depends on both space and time. The quasi-one-dimensional Euler equations (25–27) are then linearized:

$$\frac{\partial}{\partial t}\left(\frac{\rho'}{\bar{\rho}}\right) + \bar{u}\frac{\partial}{\partial x}\left(\frac{\rho'}{\bar{\rho}} + \frac{u'}{\bar{u}}\right) = 0 \tag{28}$$

$$\frac{\partial}{\partial t}\left(\frac{u'}{\bar{u}}\right) + \bar{u}\frac{\partial}{\partial x}\left(\frac{u'}{\bar{u}}\right) + \left(\frac{\rho'}{\bar{\rho}} + 2\frac{u'}{\bar{u}}\right)\frac{\mathrm{d}\bar{u}}{\mathrm{d}x} = \frac{p'}{\bar{p}}\frac{\mathrm{d}\bar{u}}{\mathrm{d}x} - \frac{\bar{p}}{\bar{\rho}\,\bar{u}}\frac{\partial}{\partial x}\left(\frac{p'}{\bar{p}}\right) \tag{29}$$

$$\left(\frac{\partial}{\partial t} + \bar{u}\frac{\partial}{\partial x}\right)\left(\frac{s'}{c_v}\right) = 0 \tag{30}$$

Introducing the mean velocity $\bar{u}$ and density $\bar{\rho}$ allows us to completely hide the section changes $A(x)$ in Eqs. (28–30). For the present approach, entropy waves have not been taken into account, even though the interaction of entropy waves with nozzles can be a source of instabilities [17,21,22]. Because combustion is a strong

[¶]Marble and Candel [17] presented an analytical resolution for a finite length choked nozzle in which the mean axial velocity varies linearly along the duct. This last approximation provides the impedance throughout the nozzle. Nevertheless, in general, the mean velocity evolution is not linear and the acoustic problem must be solved numerically.

Table 1 Reflection coefficients depending on the acoustic boundary conditions and the flow regime in the low-frequency limit

	Diffuser	Distributor
	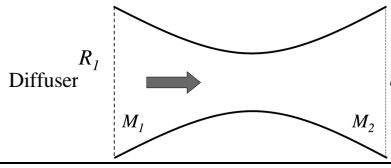	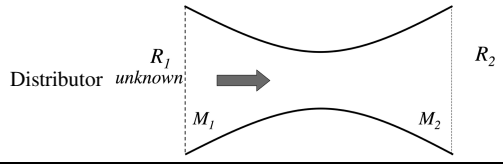
Choked	$R_2 = \frac{1-\gamma\bar{M}_2+(\gamma-1)\bar{M}_2^2}{1+\gamma\bar{M}_2+(\gamma-1)\bar{M}_2^2}$	$R_1 = \frac{1-\frac{1}{2}(\gamma-1)\bar{M}_1}{1+\frac{1}{2}(\gamma-1)\bar{M}_1}$ or $Z_1 = \frac{2}{\bar{M}_1(\gamma-1)}$
Unchoked	R_2: see Eq. (23); T_2: see Eq. (24)	R_1: see Eq. (21); T_1: see Eq. (22)

source of entropy perturbations, it is logical to assume that these waves participate in some combustion instabilities. Some recent studies, however, suggest that the entropy waves have a limited influence on the resonant modes in swirled combustors [25]. Even though this simplification may not be justified for all cases, it was used in the present study and may have to be relaxed for future work. We thus consider that entropy fluctuations are zero:

$$\frac{p'}{\gamma\bar{p}} - \frac{\rho'}{\bar{\rho}} = \frac{s'}{c_p} = 0 \quad \text{so that} \quad \frac{\rho'}{\bar{\rho}} = \frac{p'}{\gamma\bar{p}} \tag{31}$$

Under the assumption of monochromatic fluctuations, one can write

$$\begin{aligned} &\frac{p'}{\bar{p}} = \varphi(x)e^{-i\omega t}; \qquad \frac{u'}{\bar{u}} = v(x)e^{-i\omega t}; \\ &\frac{\rho'}{\bar{\rho}} = \delta(x)e^{-i\omega t} = \frac{1}{\gamma}\varphi(x)e^{-i\omega t} \end{aligned} \tag{32}$$

Using Eqs. (28), (29), and (31) and introducing the local Mach number, system (28) and (29) for the perturbed pressure φ and velocity v becomes

$$-i\omega\varphi + \bar{u}\frac{\mathrm{d}\varphi}{\mathrm{d}x} + \gamma\bar{u}\frac{\mathrm{d}v}{\mathrm{d}x} = 0 \tag{33}$$

$$\frac{\bar{u}}{\bar{M}^2}\frac{\mathrm{d}\varphi}{\mathrm{d}x} + \gamma\bar{u}\frac{\mathrm{d}v}{\mathrm{d}x} - (\gamma-1)\frac{\mathrm{d}\bar{u}}{\mathrm{d}x}\varphi + \gamma\left[2\frac{\mathrm{d}\bar{u}}{\mathrm{d}x} - i\omega\right]v = 0 \tag{34}$$

Introducing Eq. (33) in Eq. (34) also gives the momentum equation:

$$\left(\frac{1}{\bar{M}^2} - 1\right)\bar{u}\frac{\mathrm{d}\varphi}{\mathrm{d}x} - \left[(\gamma-1)\frac{\mathrm{d}\bar{u}}{\mathrm{d}x} - i\omega\right]\varphi + \gamma\left[2\frac{\mathrm{d}\bar{u}}{\mathrm{d}x} - i\omega\right]v = 0 \tag{35}$$

Using reduced values, the acoustic impedance can be written

$$Z = \frac{1}{\gamma\bar{M}}\frac{\varphi}{v} \tag{36}$$

Equations (33) and (35) can be solved if appropriate boundary conditions are specified as described subsequently. It should be noted here that only longitudinal acoustic modes are considered in this resolution, whereas higher-order acoustic modes can occur in a duct [6]. Nevertheless, because the main context is the study of the thermoacoustic stability of a combustion chamber (especially gas turbines), only the lower-frequency acoustic eigenmodes (hence longitudinal ones) are of interest.

B. Impedance of a Choked Nozzle

Distributors are most often choked in gas turbines (except for idle operating conditions). In this particular case, knowing the mean flow is enough to determine the inlet acoustic impedance of a choked nozzle. In the time domain, system (33–35) is strictly hyperbolic (terms in $-i\omega$ are replaced by time derivatives) and its two characteristic velocities (eigenvalues) are

$$\left(\frac{\mathrm{d}x}{\mathrm{d}t}\right)_{\mathcal{A}^\pm} = \bar{u} \pm \bar{c} \tag{37}$$

At the throat of a choked nozzle, $\bar{u}_* = \bar{c}_*$, which implies that the $\mathcal{A}^-$ wave does not move at the throat: no information can propagate upstream of the throat. Mathematically, it means that $x = x_*$ is a singular location for system (33–35). Equation (35) at the throat with $M^* = 1$ allows us to write the throat impedance:**

$$Z_* = \frac{1}{\gamma\bar{M}_*}\frac{\varphi_*}{v_*} = \frac{2(\mathrm{d}\bar{u}/\mathrm{d}x)|_* - i\omega}{(\gamma-1)(\mathrm{d}\bar{u}/\mathrm{d}x)|_* - i\omega} \tag{38}$$

C. Numerical Resolution

To determine inlet or outlet acoustic impedance of ducts, the mean flow needs to be characterized first. Its computation within a nozzle of cross section $A(x)$ is a simple textbook problem; because $\bar{M} = \bar{u}/\bar{c}$ is the local Mach number, one can write, using Hugoniot relations derived from Eqs. (25–27) for stationary flow,

$$\frac{A(x)}{A_*} = \frac{1}{\bar{M}}\left[\frac{2}{\gamma+1}\left(1 + \frac{\gamma-1}{2}\bar{M}^2\right)\right]^{\frac{\gamma+1}{2(\gamma-1)}} \tag{39}$$

The Mach number is supposed to be 1 at $x = x_*$. Knowing $\bar{M}$ at a boundary section enables us to calculate the critical section A_*. Then the Mach number can be determined everywhere else using an iterative Newton–Raphson method for Eq. (39). All other variables can be calculated with isentropic flow relations using total values:

$$\frac{\bar{\rho}(x)}{\bar{\rho}_t} = \left(1 + \frac{\gamma-1}{2}\bar{M}^2\right)^{\frac{-1}{\gamma-1}} \quad \text{and} \quad \frac{\bar{p}(x)}{\bar{p}_t} = \left(1 + \frac{\gamma-1}{2}\bar{M}^2\right)^{\frac{-\gamma}{\gamma-1}} \tag{40}$$

Knowing the mean flow, the impedance can be computed as follows. For a given time frequency ω, the computational domain is discretized in space $x = \{x^{(j)}\}_{1\le j\le N}$ and the system (33–35) becomes

$$-i\omega\varphi^{(j)} + \frac{\bar{u}^{(j)}}{h}\delta_\epsilon^-\varphi^{(j)} + \gamma\frac{\bar{u}^{(j)}}{h}\delta_\epsilon^- v^{(j)} = 0 \tag{41}$$

$$\left(\frac{1}{(\bar{M}^{(j)})^2} - 1\right)\frac{\bar{u}^{(j)}}{h}\delta_\epsilon^-\varphi^{(j)} - \left[\frac{(\gamma-1)}{h}\Delta_0^\epsilon\bar{u}^{(j)} - i\omega\right]\varphi^{(j)} + \gamma\left[\frac{2}{h}\Delta_0^\epsilon\bar{u}^{(j)} - i\omega\right]v^{(j)} = 0 \tag{42}$$

where the difference operators Δ_0^ϵ and δ_ϵ^- are defined by

$$\delta_\epsilon^-\varphi^{(j)} = \epsilon(\varphi^{(j)} - \varphi^{(j-1)}) \quad \text{and} \quad \Delta_0^\epsilon\bar{u}^{(j)} = \frac{\epsilon}{2}(\bar{u}^{(j+1)} - \bar{u}^{(j-1)}) \tag{43}$$

The parameter ϵ depends on the type of flow: for a diffuser, $\epsilon = 1$, whereas for a distributor, $\epsilon = -1$. System (41) and (42) is integrated from where the impedance is given [$x = x^{(1)}$] to where it is searched ($x = x^{(N)}$), as shown in Fig. 4. The system can thus be written in compact form:

**For low pulsations and constant section, Eqs. (33) and (35) reduce to Marble and Candel's [17] result [Eq. (15)]. In this case, Eqs. (33) and (35) lead to $\mathrm{d}\varphi/\mathrm{d}x = \gamma(\mathrm{d}v/\mathrm{d}x)$, so that $\varphi = \varphi_*$ and $v = v_*$, and the impedance at the inlet is $Z_1 = (1/\gamma\bar{M}_1)(\varphi_1/v_1) = (1/\gamma\bar{M}_1)(\varphi_*/v_*)$. At the throat for $\omega \to 0$, Eq. (38) gives $Z_* = 2/(\gamma-1)$, $\varphi_*/v_* = 2\gamma/(\gamma-1)$, and $Z_1 = 2/[(\gamma-1)\bar{M}_1]$, which is Eq. (38).

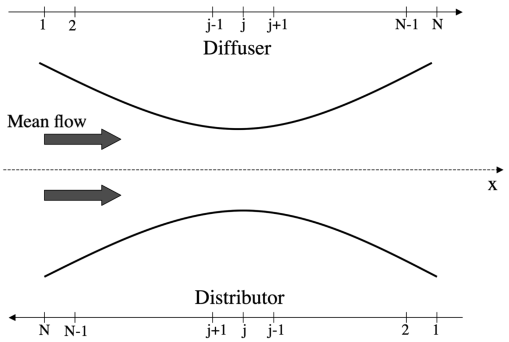

Fig. 4 System (41) and (42) integration for diffusers and distributors. Boundary conditions are given at $x = x^{(N)}$.

$$[D]^{(j)} \begin{pmatrix} \varphi^{(j)} \\ \nu^{(j)} \end{pmatrix} = \begin{pmatrix} g_1(\varphi^{(j-1)}) \\ g_2(\nu^{(j-1)}) \end{pmatrix} \tag{44}$$

where $[D]^{(j)}$ is a 2×2 matrix and the acoustic impedance can be expressed at $x = x^{(j)}$:

$$Z^{(j)} = \frac{1}{\gamma \bar{M}^{(j)}} \frac{\varphi^{(j)}}{\nu^{(j)}} \tag{45}$$

At $x = x^{(1)}$, only $Z = Z^{(1)}$ is known; typically, section 1 must be the throat for choked flows or a section in which Z is known.[††] System (44) with Eq. (45) is solved as follows. In the section in which the impedance is known, $\nu^{(1)}$ is set equal to a constant $K \neq 0$ so that $(\varphi^{(1)}, \nu^{(1)})^T = (\gamma M Z^{(1)} K, K)^T$, which is a set of boundary conditions for system (44). From node to node, $\forall\ j \in \{2, \ldots, N\}$, $[D]^{(j)}$ can be inverted to give $(\varphi^{(N)}, \nu^{(N)})^T$. $Z^{(N)}$ is then recovered, again using Eq. (45). Of course, due to the linearity of Eqs. (33) and (35), the choice of K has no effect on $Z^{(N)}$, as pointed out by Mani [26]. Calculation is repeated for several frequencies to obtain the impedance curve versus frequency $Z^{(N)}(\omega)$.

IV. Numerical Evaluation of Impedance Using the Euler Equations

Another way to determine acoustic impedances of section-varying ducts is to use a space–time solver and the Euler equation without linearization; extracting acoustic waves from the solution of the unsteady Euler equations is expensive but is used here as a verification of the FD method of Sec. III. The solver here is based on the cell-vertex finite volume formulation of the Lax–Wendroff scheme [27,28], and boundary conditions are computed following the Euler characteristic boundary-condition approach [29,30]. For example, the time simulation is solved for a distributor (Fig. 5) as follows. The mean flow is first imposed in the duct. When the mean flow is established, monochromatic acoustic waves $\mathcal{A}^+$ of angular frequency ω are injected at the inlet (respectively, outlet) of the computational domain. The outlet impedance is set to Z_2. The reflected waves $\mathcal{A}^-$ are then extracted from the pressure and velocity temporal signals at the inlet, using a characteristic decomposition. Finally, a Fourier analysis of ingoing (reference) and outgoing acoustic waves gives the real and imaginary parts of the inlet acoustic impedance at angular frequency ω.

This operation is repeated for several angular frequencies to obtain a map of $Z(\omega)$. Care has to be taken with the use of the inlet boundary condition, because it must impose both the mean flow and an acoustic wave [31]. Moreover, it must totally evacuate the reflected waves $\mathcal{A}^-$ (nonreflecting inlet boundary condition), otherwise the calculation of the inlet impedance is biased. In the following comparisons, only the case of the distributor is shown, even though validations have also been made for diffusers. The procedure is similar for diffusers,

[††]In the case of a choked distributor, the singularity is avoided by using relation (38) as the boundary condition for system (44), writing $x^{(1)} = x_*$ and $Z^{(1)} = Z_*$.

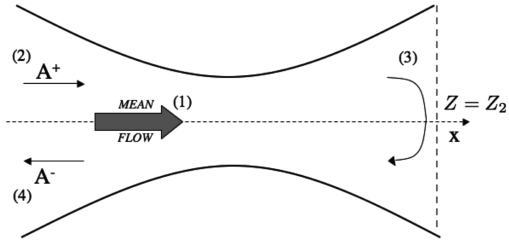

Fig. 5 Impedance calculation with a temporal solver: once the mean flow is stabilized (1), downstream traveling acoustic waves $\mathcal{A}^+$ are injected at the inlet (2) and compared with the reflected acoustic waves $\mathcal{A}^-$ that come back (3)–(4).

except that the inlet impedance Z_1 is imposed and the outlet impedance Z_2 is calculated.

V. Code Verification

The FD method described in Sec. III.C is validated here in two cases: a constant-section duct in which an analytical solution is available (Sec. V.A) and a distributor (unchoked) with a fixed outlet pressure in which a space–time solver (Sec. IV) is used to evaluate the impedance by forcing the inlet in the time domain (Sec. V.B).

A. Comparison of the FD Method and Analytical Formulas in a Constant-Section Duct

For simple test cases as the constant-section duct, a trivial analytical solution can be derived. The acoustic pressure and velocity of nonzero Mach number flow in a constant-section duct of length L both verifiy

$$\frac{\mathrm{d}^2\phi}{\mathrm{d}t^2} - \tilde{c}^2 \frac{\partial^2 \phi}{\partial x^2} = 0 \tag{46}$$

where $\phi = \phi(x, t)$ is either p' or u' and $\mathrm{d}/\mathrm{d}t = \partial/\partial t + \bar{u}\partial/\partial x$. The solutions of Eq. (46) are given by Eqs. (2) and (3) (Sec. II). Given the impedance at the outlet of the duct, one can write it at the inlet for $\bar{M} < 1$. It was calculated for flow conditions summarized in Table 2 and outlet impedances $Z_2 = 0$ and ∞.

The analytical formulations of inlet impedance in those two cases are the following:

$$Z_1|_{Z_2=0} = -i \tan\left(\frac{kL}{1 - \bar{M}^2}\right) \tag{47}$$

$$Z_1|_{Z_2=\infty} = i \cot\left(\frac{kL}{1 - \bar{M}^2}\right) \tag{48}$$

Comparisons between imaginary parts of inlet impedances (real parts are zero) given by the FD method and Eqs. (47) and (48) are shown in Figs. 6 and 7 for a frequency range from 1 to 1000 Hz. The agreement between the two methods is very good even for higher frequencies.

B. Comparison of All Methods for an Unchoked Distributor

The comparison between the different methods to calculate impedances is performed here for an unchoked distributor. The geometry (Fig. 8) is discretized using a nonregular Cartesian grid for the Euler equations solver, and the characteristics of the flow are gathered in Table 3. The outlet impedance at $x = L_x$ is set to $Z_2 = 0$.

Figure 9 shows good agreement between the results of the space–time solver Euler equations solver and Eq. (39) for the mean flow in the distributor, characterized here by a y-integrated Mach number:

$$\bar{M}(x) = \int_{L_y} \bar{M}(x, y)\, \mathrm{d}y$$

Real and imaginary parts of inlet acoustic impedance are plotted in Figs. 10 and 11. Here again, the agreement between the FD method and the space–time solver is good. Moreover, the asymptotic

Table 2 Main parameters of the flow in the 1-D tube

Parameters	Value
L	0.2
ρ	1.1723
$r = R/W_{\text{air}}$	288.19
T	300
M	0.2

Table 3 Characteristics of the variable-section duct and boundary conditions

Geometry	Value	Boundary conditions	Value
L_x	0.2	u_{in}	30
L_y (inlet)	0.015	p_{out}	1.013
N_x	101	ρ_{in}	1.1723
N_y	11	T_{in}	300
γ	1.399	$r = R/W_{\text{air}}$	288.19

behavior at low frequencies for both approaches coincides with the impedance analytically obtained from Eq. (21). Nevertheless, as in the case of a constant-section duct, the real and imaginary parts of the impedance quickly evolve with frequency. It clearly shows a posteriori the importance of solving system (44) and the limits of analytical formulas (such as those obtained in Sec. II). The peaks observed on the real part (and change of sign of the imaginary part) correspond to the acoustic modes of the nozzle. The first one is the quarter-wave mode $\lambda = 4L_x$ and $f = 435$ Hz. Figures 12 and 13 show that the low-frequency approximation [Eq. (21)] is valid up to frequencies f of approximately 200 Hz and a wavelength $\lambda \approx 1.7$ m $\approx 10L_x$. Note that the real part of the inlet impedance is negative for some range of frequencies. This is equivalent to a reflection-coefficient modulus greater than 1. It is possible because of the presence of a mean flow, as pointed out by Munjal [32] and Mechel et al. [33]. In such a case, the average flux through a surface and over a period of a fluctuation is written

$$W_{\text{ac}} = \frac{|\mathcal{A}^I|^2}{2\bar{\rho}\,\bar{c}}[(1+M)^2 - |R|^2(1-M)^2] \tag{49}$$

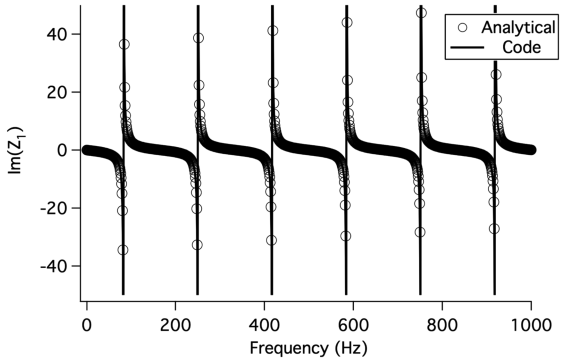

Fig. 6 Comparison between inlet impedances given by the analytical expression (47) and the FD method. The outlet impedance is $Z_2 = 0$.

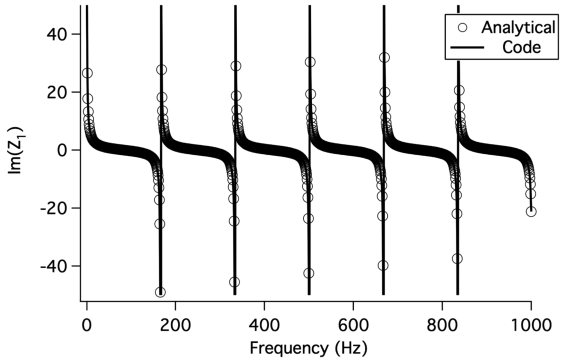

Fig. 7 Comparison between inlet impedances given by the analytical expression (48) and the FD method. The outlet impedance is $Z_2 = \infty$.

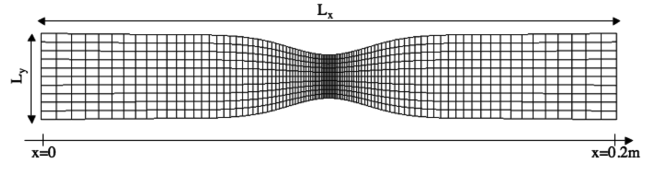

Fig. 8 Geometry and mesh of the variable-section duct.

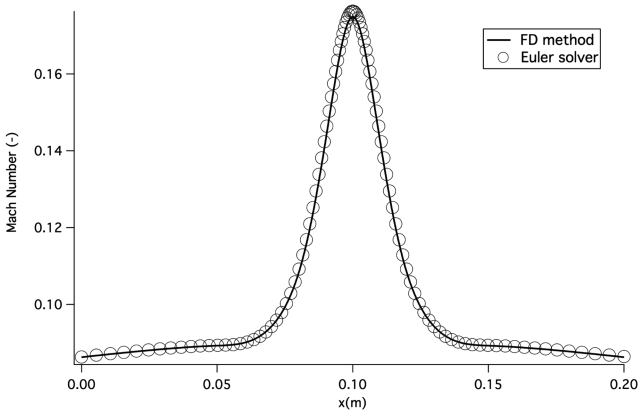

Fig. 9 Mean Mach number evolution; $\bar{M}(x) = \int_{L_y} \bar{M}(x,y)\mathrm{d}y$.

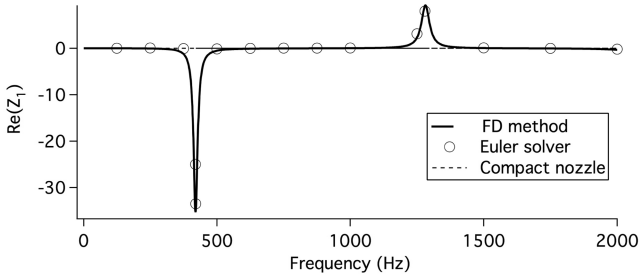

Fig. 10 Real part of the inlet acoustic impedance for the nozzle of Fig. 8.

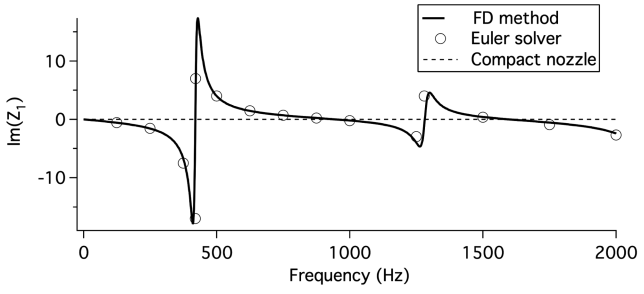

Fig. 11 Imaginary part of the inlet acoustic impedance for the nozzle of Fig. 8.

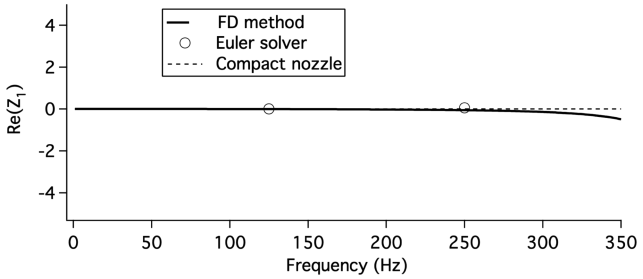

Fig. 12 Zoom of the real part of the inlet acoustic impedance of the variable-section duct described, corresponding to the black box in Fig. 10.

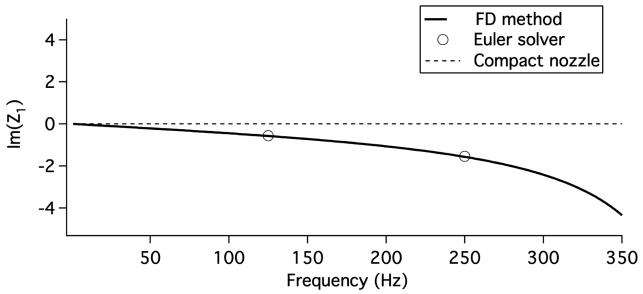

Fig. 13 Zoom of the imaginary part of the inlet acoustic impedance of the variable-section duct described, corresponding to the black box in Fig. 11.

Equation (49) shows that W_{ac} can be positive (acoustic loss) even if $|R| > 1$, as soon as there is a mean flow ($M \neq 0$).[‡‡]

VI. Impedances of Combustion Chambers in Gas Turbines

As recalled in Sec. II, it is common to set $Z = 0$ for a flow that discharges in the atmosphere. In addition, $Y = 0$ is also often used for the inlet of a duct in which the mass flow rate is imposed constant in time. These boundary conditions can be used in the case of academic configurations but not in gas turbines, in which distributors and diffusers must be taken into account. The previous sections have shown that methods exist to evaluate the inlet impedance of distributors or the outlet impedances of diffusers when the impedance of the other side of the nozzle is known. The most favorable case is when the ducts connected to the casing or the chamber are choked. Indeed, the impedance at location $x = x^{(1)}$ is known. As shown in Sec. III, the impedance at the throat of a choked distributor can be expressed through relation (38). For a choked diffuser, a normal shock (or a shock network) exists between the throat and the casing inlet. Then, relations derived by Stow et al. [21] and Moase et al. [22] can be used to determine the reflection coefficient of the shock.

Unfortunately, diffusers and distributors are not always choked and the flow can be fully subsonic, especially at idle regimes. In such cases, location $x = x^{(1)}$, where the calculation using FD method is started, is often the inlet or the outlet of a rotating machine. A first approximation is to use $Y^{(1)} = 0$ at the inlet of the diffuser (to model a constant flow rate) or $Z^{(1)} = 0$ at the outlet of the distributor (to model a constant pressure), but those are crude approximations. Because the accuracy of the resolution of Eq. (44) strongly relies on those values, one would also rather try to model the compressor and the turbine with complex impedances by studying their acoustic response. This could be done using the work of Kaji and Okazaki [34] (and the concept of a semi-actuator disk), if little information on the turbomachinery blade rows is provided. A finer way to determine complex impedances of turbomachines lying upstream and downstream of the chamber is to experimentally measure or compute the scattering of acoustic waves through them [35,36].

The next section shows the effects of impedance changes for diffusers and distributors in the case of a realistic gas turbine. It confirms their importance and the necessity of modeling them accurately.

VII. Application of Impedance Methods in a Helmholtz Solver for a Real Chamber

This section shows how Helmholtz solvers are built and provides one example of real gas turbine application in which the result of the solver is directly controlled by the acoustic impedances used at inlets and outlets. Multidimensional Helmholtz codes [12,37–39] solve the linearized acoustic-wave equation in the Fourier domain: they give the complex frequency (stability analysis) and spatial structure of all acoustic eigenmodes.

The Helmholtz equation is obtained by linearizing the reactive Navier–Stokes equations under the following assumptions [3,39]: low Mach number, no volume forces, linear acoustics, large-scale fluctuations (long wavelength), homogeneous mean pressure, and constant polytropic coefficient γ. The fluctuating pressure field is then given by the wave equation[§§]

$$\nabla \cdot (c^2 \nabla p') + \omega^2 p' = 0 \tag{50}$$

with the following boundary conditions:

$$Z(\omega) = \frac{i\omega}{\bar{c}} \frac{p'}{\nabla p' \cdot \mathbf{n}} \tag{51}$$

where $Z(\omega)$ is the local impedance on the domain boundaries. System (50) and (51) is discretized using finite element formulation [39] as follows. To be able to handle complex geometries such as gas turbine combustors, the computational domain is decomposed in linear P1 elements (triangles in 2-D, tetrahedra in 3-D) and Eqs. (50) and (51) are solved using a lumped mass matrix Galerkin finite element method (see Nicoud et al. [15]). The discretized equation can be put in a matrix form:

$$[A]\{p'\} + \omega[B(\omega)]\{p'\} + \omega^2[C]\{p'\} = 0 \tag{52}$$

where $[B(\omega)]$ contains boundary conditions. Matrix problem (52) is a nonlinear eigenvalue problem and is reformulated to be linear. It is then solved using a parallelized implementation of the Arnoldi method [40]. Several examples of its application have already been referenced [12,13,15] and show the accuracy of the solver.

Compared with Navier–Stokes solvers in the space–time domain, Helmholtz codes are faster and directly supply the frequency and structure of all acoustic modes. Moreover, these codes can easily handle complex-valued boundary conditions that vary with frequency, whereas it remains a challenge in the time domain, especially in complex geometries, despite some developments [41–43] making use of discrete convolutions.

As an example, to show the influence of the boundary conditions, several calculations were realized on a real annular combustor (see Figs. 14 and 15). In this configuration, both the chamber and its casing are considered and the swirler is also meshed. The only differences between the computations presented next are the acoustic boundary conditions at the chamber inlet and outlet (which are, respectively, linked with the diffuser and the distributor). The boundary conditions are either obtained using the analytical formulas of Table 1 or computed using the FD method of Sec. III.

For the diffuser, the boundary condition upstream of the throat is supposed to be either $Z_{1,in} = 0$ or $Y_{1,in} = 0$ (Fig. 15). For the

[‡‡]As indicated by Munjal [32], this paradox ($|R| > 1$) is only apparent due to the choice of the variables u' and p' to define the reflection coefficient in Eq. (5). If proper aeroacoustic variables adapted to nonzero mean flow are used to define R (the perturbed mass flow rate $\dot{m}'$ and the perturbed total enthalpy h_t'), the reflection coefficient is always less than 1.

[§§]For this example, the effects of the active flame on the pressure field are neglected [6,39].

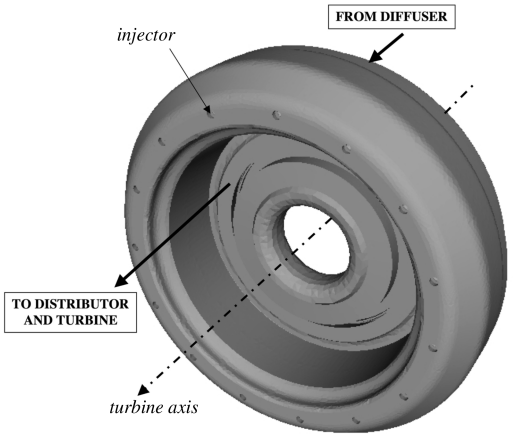

Fig. 14 Geometry of the complete annular combustor.

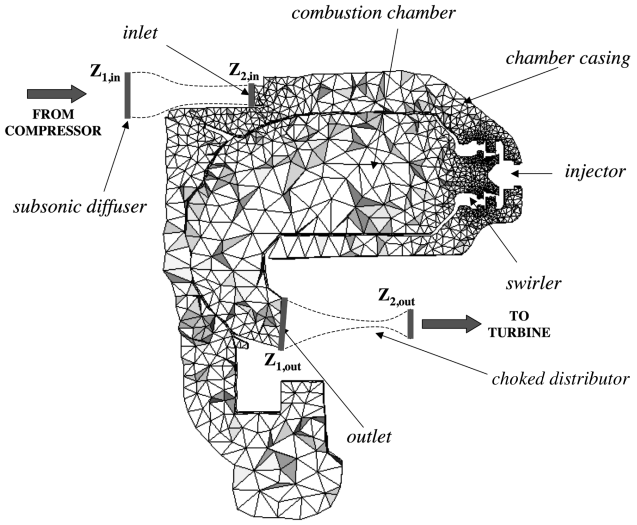

Fig. 15 Cut of the mesh used for the acoustic eigenmode calculation.

distributor, the acoustic condition downstream of the nozzle corresponds either to $Z_{2,\text{out}} = \infty$ or to a $Z_{2,\text{out}} = Z_*$ choked nozzle. Figures 16 and 17 show $Z_{2,\text{in}}$ and $Z_{1,\text{out}}$, calculated with the FD method, with $Y_{1,\text{in}} = 0$ and $Z_{2,\text{out}} = Z_*$. The results of the Helmholtz code are limited here to the first mode (lowest frequency). Table 4 provides the frequency of this first mode for each case. The structures of the modes (adimensionalized pressure modulus in the central plane of the chamber) are displayed in Figs. 18 and 19. The results of the calculation illustrates the effects of impedances on the results. A comparison between cases A and B highlights the impact of the inlet boundary condition on the diffuser side. Both the structure of the mode and its frequency (that has shifted from 245 to 360 Hz) are modified when the inlet impedance varies from 0 (case A) to ∞ (case B). The approximation of $u' = 0$ (infinite impedance) for the outlet to model a choked nozzle (case B) gives very similar results to the right acoustic impedance calculated using the FD solver (case C), at least for low frequencies. Analytical formulas or impedances given by the FD method (case D) should be preferred because the frequency and structure of the first mode depend strongly on their values.

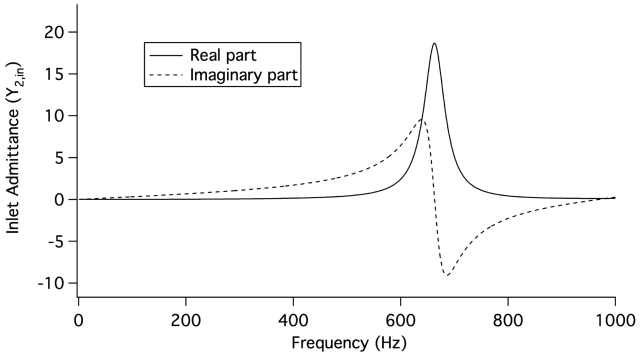

Fig. 16 Reduced acoustic admittance $Y_{2,\text{in}} = 1/Z_{2,\text{in}}$ at the outlet of the diffuser.

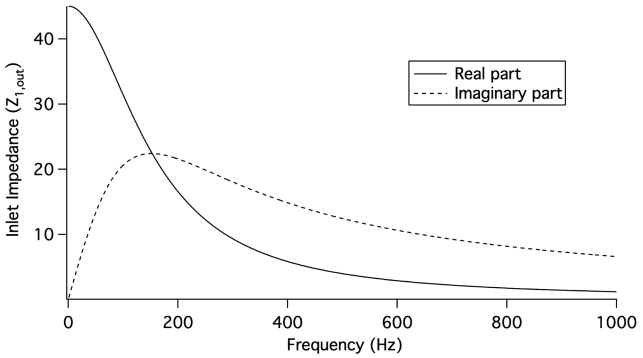

Fig. 17 Reduced acoustic impedance $Z_{1,\text{out}}$ at the inlet of the distributor.

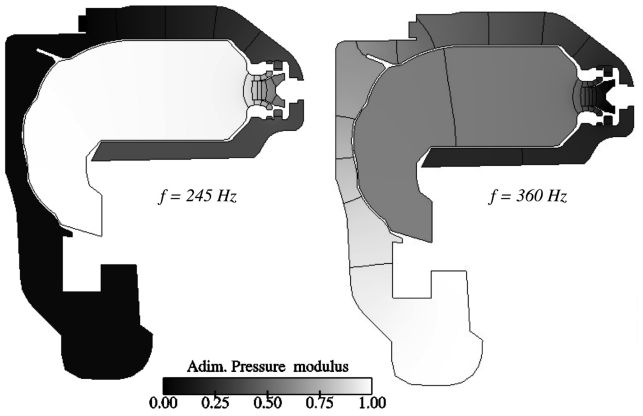

Fig. 18 First longitudinal acoustic eigenmode for two different inlet boundary conditions; case A (left): $p' = 0$ at the inlet and $u' = 0$ at the outlet and case B (right): $u' = 0$ at the inlet and $u' = 0$ at the outlet.

VIII. Conclusions

To determine the acoustic eigenmodes of gas turbine combustors, Helmholtz solvers are a very interesting and commonly used method [2,4,5,14,15]. This paper shows that their accuracy directly depends on the boundary conditions used for inlets and outlets. Some

Table 4 Frequencies of the first acoustic eigenmode and set of boundary conditions used for the calculations

Cases	Inlet impedance $Z_{2,\text{in}}$	Outlet impedance $Z_{1,\text{out}}$	First mode frequency, Hz
A	0 [Eq. (23) with $M_1 \approx M_2$ and $R_1 = -1$]	∞ [Eq. (15) with $M_1 \to 0$]	245
B	∞ [Eq. (23) with $M_1 \approx M_2$ and $R_1 = 1$]	∞ [Eq. (15) with $M_1 \to 0$]	360
C	∞ [Eq. (23) with $M_1 \approx M_2$ and $R_1 = 1$]	$Z_{1,\text{out}}$ (FD method)	357
D	$Z_{2,\text{in}}$ (FD method)	$Z_{1,\text{out}}$ (FD method)	330

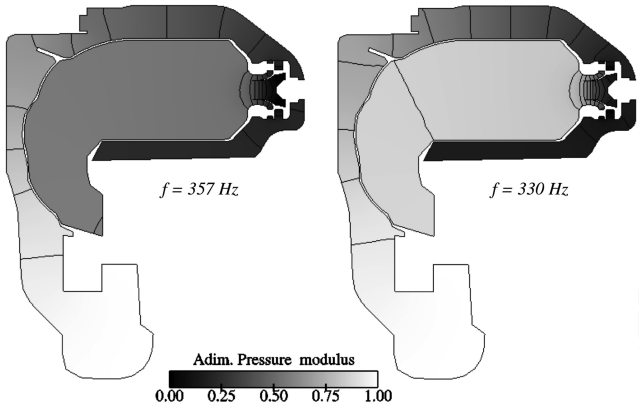

Fig. 19 First longitudinal acoustic eigenmode for two different simulations; case C (left): $u' = 0$ at the inlet and $Z_{1,\text{out}}$ is given by the FD method at the outlet and cases D (right): $Z_{2,\text{in}}$ at the inlet $Z_{1,\text{out}}$ at the outlet are both computed using the FD solver.

analytical expressions have been derived in the past [17], extended here, and shown to be efficient at low frequencies. In practical cases, they are not often sufficient. A methodology to calculate those acoustic boundary conditions, by approximating the ducts connected to the chamber as one-dimensional nozzles and solving linearized Euler equations, was presented and verified with different academic cases, including a comparison with a full Euler equations solver. It enables the quick determination of inlet or outlet impedances of section-varying ducts (choked or not) in the frequency domain. The application of this method in a realistic gas turbine chamber with a subsonic diffuser and a choked distributor has shown that even when the whole chamber is computed (including casing and swirlers), results still depend on the boundary conditions used for the inlets and outlets. This means that a proper prediction of acoustic modes cannot be performed without these impedances. Results show that although impedances can be calculated on the distributor side, where a choked nozzle is usually found, the problem is more complex for the inlet in which diffusers are often unchoked and in which a location to identify a proper acoustic boundary condition is difficult to find. The study of the scattering of acoustic waves has to then be considered, to derive accurate impedances.

Acknowledgments

Financial support was supplied by the Safran group. C. Rey, O. Thual, F. Jaegle, M. Leyko, M. Myrczik, C. Sensiau, F. Nicoud, and the Energétique Moléculaire et Macroscopique, Combustion (EM2C) laboratory are thanked for questions and discussions on theoretical backgrounds. The authors are also grateful to Hans Bodén and the referees for their pertinent remarks and the references they supplied.

References

[1] Lieuwen, T., and Yang, V., "Combustion Instabilities in Gas Turbine Engines: Operational Experience, Fundamental Mechanisms and Modeling," *Progress in Astronautics and Aeronautics*, Vol. 210, AIAA, Reston, VA, 2005.

[2] Culick, F., "Combustion Instabilities in Liquid-Fueled Propulsion Systems: An Overview," AGARD 72B PEP meeting, 1987.

[3] Crighton, D., Dowling, A., Ffowcs Williams, J., Heckl, M., and Leppington, F., *Modern Methods in Analytical Acoustics*, Lecture Notes, Springer-Verlag, New York, 1992.

[4] Dowling, A., "The Calculation of Thermoacoustic Oscillations," *Journal of Sound and Vibration*, Vol. 180, No. 4, 1995, pp. 557–581. doi:10.1006/jsvi.1995.0100

[5] Polifke, W., Poncet, A., Paschereit, C., and Doebbeling, K., "Reconstruction of Acoustic Transfer Matrices by Instationary Computational Fluid Dynamics," *Journal of Sound and Vibration*, Vol. 245, No. 3, 2001, pp. 483–510. doi:10.1006/jsvi.2001.3594

[6] Poinsot, T., and Veynante, D., *Theoretical and Numerical Combustion*, 2nd ed., R. T. Edwards, Philadelphia, 2005.

[7] Colin, O., Ducros, F., Veynante, D., and Poinsot, T., "A Thickened Flame Model for Large Eddy Simulations of Turbulent Premixed Combustion," *Physics of Fluids*, Vol. 12, No. 7, 2000, pp. 1843–1863. doi:10.1063/1.870436

[8] Angelberger, C., Egolfopoulos, F., and Veynante, D., "Large Eddy Simulations of Chemical and Acoustic Effects on Combustion Instabilities," *Flow, Turbulence and Combustion*, Vol. 65, No. 2, 2000, pp. 205–222. doi:10.1023/A:1011477030619

[9] Pitsch, H., and Duchamp de la Geneste, L., "Large Eddy Simulation of Premixed Turbulent Combustion Using a Level-Set Approach," *Proceedings of the Combustion Institute*, Vol. 29, No. 2, 2002, pp. 2001–2005. doi:10.1016/S1540-7489(02)80244-9

[10] Pierce, C., and Moin, P., "Progress-Variable Approach for Large Eddy Simulation of Nonpremixed Turbulent Combustion," *Journal of Fluid Mechanics*, Vol. 504, Apr. 2004, pp. 73–97. doi:10.1017/S0022112004008213

[11] Roux, S., Lartigue, G., Poinsot, T., Meier, U., and Bérat, C., "Studies of Mean and Unsteady Flow in a Swirled Combustor Using Experiments, Acoustic Analysis and Large Eddy Simulations," *Combustion and Flame*, Vol. 141, Nos. 1–2, 2005, pp. 40–54. doi:10.1016/j.combustflame.2004.12.007

[12] Martin, C., Benoit, L., Sommerer, Y., Nicoud, F., and Poinsot, T., "LES and Acoustic Analysis of Combustion Instability in a Staged Turbulent Swirled Combustor," *AIAA Journal*, Vol. 44, No. 4, 2006, pp. 741–750. doi:10.2514/1.14689

[13] Selle, L., Benoit, L., Poinsot, T., Nicoud, F., and Krebs, W., "Joint Use of Compressible Large-Eddy Simulation and Helmoltz Solvers for the Analysis of Rotating Modes in an Industrial Swirled Burner," *Combustion and Flame*, Vol. 145, Nos. 1–2, 2006, pp. 194–205. doi:10.1016/j.combustflame.2005.10.017

[14] Krebs, W., Walz, G., and Hoffmann, S., "Thermoacoustic Analysis of Annular Combustor," 5th AIAA Aeroacoustics Conference, Bellevue, WA, AIAA Paper 99-1971, 1999.

[15] Nicoud, F., Benoit, L., and Sensiau, C., "Acoustic Modes in Combustors with Complex Impedances and Multidimensional Active Flames," *AIAA Journal*, Vol. 45, No. 2, 2007, pp. 426–441. doi:10.2514/1.24933

[16] Eldredge, J. D., and Dowling, A. P., "The Absorption of Axial Acoustic Waves by a Perforated Liner with Bias Flow," *Journal of Fluid Mechanics*, Vol. 485, May 2003, pp. 307–355. doi:10.1017/S0022112003004518

[17] Marble, F., and Candel, S., "Acoustic Disturbances from Gas Nonuniformities Convected Through a Nozzle," *Journal of Sound and Vibration*, Vol. 55, 1977, pp. 225–243. doi:10.1016/0022-460X(77)90596-X

[18] Candel, S., "Etudes Théoriques et Expérimentales de la Propagation Acoustique en Milieu Inhomogène et en Mouvement," Ph.D. Thesis, Univ. Paris VI, Paris, 1977.

[19] Moase, W., Brear, M., and Manzie, C., "Linear and Nonlinear Acoustic Behaviour of Outlet Nozzles," *Proceedings of the Fifteenth Australasian Fluid Mechanics Conference* [CD-ROM], edited by M. Behnia, W. Lin, and G. D. McBain, Paper AFMC00184, Univ. of Sydney, Sydney, Australia, 2004.

[20] Rienstra, S., "A Small Strouhal Number Analysis for Acoustic Wave-Jet Flow-Pipe Interaction," *Journal of Sound and Vibration*, Vol. 86, No. 4, 1983, pp. 539–556. doi:10.1016/0022-460X(83)91019-2

[21] Stow, S. R., Dowling, A. P., and Hynes, T. P., "Reflection of Circumferential Modes in a Choked Nozzle," *Journal of Fluid Mechanics*, Vol. 467, Sept. 2002, pp. 215–239. doi:10.1017/S0022112002001428

[22] Moase, W., Brear, M., and Manzie, C., "The Forced Response of Choked Nozzles and Supersonic Diffusers," *Journal of Fluid Mechanics*, Vol. 585, Aug. 2007, pp. 281–304. doi:10.1017/S0022112007006647

[23] Tsien, H., "The transfer Functions of Rocket Nozzles," *Journal of the American Rocket Society*, Vol. 22, 1952, pp. 139–143.

[24] Crocco, L., Monti, R., and Grey, J., "Verification of Nozzle Admittance Theory by Direct Measurement of the Admittance Parameter," *Journal of the American Rocket Society*, Vol. 31, 1961, pp. 771–775.

[25] Sattelmayer, T., "Influence of the Combustor Aerodynamics on Combustion Instabilities from Equivalence Ratio Fluctuations," *Journal of Engineering for Gas Turbines and Power*, Vol. 125, No. 1, 2003, pp. 11–19. doi:10.1115/1.1365159

[26] Mani, R., "Low-Frequency Sound Propagation in a Quasi-One-Dimensional Flow," *Journal of Fluid Mechanics*, Vol. 104, Mar. 1981,

pp. 81–92.
doi:10.1017/S0022112081002826
[27] Ni, R., "A Multiple-Grid Scheme for Solving the Euler Equations," *AIAA Journal*, Vol. 20, No. 11, 1982, pp. 1565–1571.
doi:10.2514/3.51220
[28] Schönfeld, T., and Rudgyard, M., "Steady and Unsteady Flows Simulations Using the Hybrid Flow Solver AVBP," *AIAA Journal*, Vol. 37, No. 11, 1999, pp. 1378–1385.
[29] Thompson, K., "Time-Dependent Boundary Conditions for Hyperbolic Systems, 2," *Journal of Computational Physics*, Vol. 89, No. 2, 1990, pp. 439–461.
doi:10.1016/0021-9991(90)90152-Q
[30] Poinsot, T., and Lele, S., "Boundary Conditions for Direct Simulation of Compressible Viscous Flows," *Journal of Computational Physics*, Vol. 101, No. 1, 1992, pp. 104–129.
doi:10.1016/0021-9991(92)90046-2
[31] Kaufmann, A., Nicoud, F., and Poinsot, T., "Flow Forcing Techniques for Numerical Simulation of Combustion Instabilities," *Combustion and Flame*, Vol. 131, No. 4, 2002, pp. 371–385.
doi:10.1016/S0010-2180(02)00419-4
[32] Munjal, M., *Acoustics of Ducts and Mufflers*, Wiley, New York, 1986.
[33] Mechel, F. P., Schiltz, W. M., and Dietz, J., "Akustische Impedanz einer Luftdurchströmten Öffnung," *Acustica*, Vol. 15, 1965, pp. 199–206.
[34] Kaji, S., and Okazaki, T., "Propagation of Sound Waves Through a Blade Row, 2: Analysis Based on Acceleration Potential Method," *Journal of Sound and Vibration*, Vol. 11, No. 3, 1970, pp. 355–375.
doi:10.1016/S0022-460X(70)80039-6
[35] Schulten, J., "Sound Generated by Rotor Wakes Interacting with a Leaned Vane Stator," *AIAA Journal*, Vol. 20, No. 10, 1982, pp. 1352–1358.
doi:10.2514/3.51195
[36] Atassi, H., Ali, A., Atassi, O., and Vinogradov, I., "Scattering of Incident Disturbances by an Annular Cascade in a Swirling Flow," *Journal of Fluid Mechanics*, Vol. 499, Jan. 2004, pp. 111–138.
doi:10.1017/S0022112003007031
[37] Nottin, C., "*Large Eddy Simulation of Combustion Instabilities*," Ph.D. Thesis, Ecole Centrale Paris, Paris, 2000.
[38] Krebs, W., Walterskötter, R., Flohr, P., Walz, G., and Hoffmann, S., "Effect of Burner Design Parameters on Thermoacoustic Stability of Annular Gas Turbine Combustors," *Acoustics of Combustion*, edited by E. Seminar, Vol. 49, Univ. of Twente, Enschede, The Netherlands, 2000.
[39] Benoit, L., "Prédiction des Instabilités Thermoacoustiques dans les Turbines à Gaz," Ph.D. Thesis, Univ. Montpellier 2, Montpellier, France, 2005.
[40] Lehoucq, R., and Sorensen, D., "ARPACK: Solution of Large Scale Eigenvalue Problems with Implicitly Restarted Arnoldi Methods," *ARPACK Users' Guide*, http://www.caam.rice.edu/software/ARPACK, 1997.
[41] Fung, K., Ju, H., and Tallapragada, B., "Impedance and Its Time-Domain Extensions," *AIAA Journal*, Vol. 38, No. 1, 2000, pp. 30–38.
[42] Fung, K., and Ju, H., "Broadband Time-Domain Impedance Models," *AIAA Journal*, Vol. 39, No. 8, 2001, pp. 1449–1454.
[43] Ju, H., and Fung, K., "Time-Domain Impedance Boundary Conditions with Mean Flow Effects," *AIAA Journal*, Vol. 39, No. 9, 2001, pp. 1683–1690.

C. Bailly
Associate Editor